Solar Energy Materials & Solar Cells 134 (2015) 400–406

Contents lists available at ScienceDirect

Solar Energy Materials & Solar Cells

journal homepage: www.elsevier.com/locate/solmat

Interfacial carrier dynamics in PbS-ZnO light harvesting assemblies and their potential implication in photovoltaic/ photocatalysis application

Samim Sardar [a], Prasenjit Kar [a], Soumik Sarkar [a], Peter Lemmens [b], S.K. Pal [a,*]

[a] Department of Chemical, Biological and Macromolecular Sciences, S. N. Bose National Centre for Basic Sciences, Block JD, Sector III, Salt Lake, Kolkata 700 098, India

[b] Institute for Condensed Matter Physics, TU Braunschweig, Mendelssohnstraße 3, 38106 Braunschweig, Germany

ARTICLE INFO

Article history:
Received 16 September 2014
Received in revised form
25 November 2014
Accepted 21 December 2014

Keywords:
PbS – ZnO nanocomposites
Light-harvesting assemblies (LHAs)
Interfacial carrier dynamics
Hole trapping
Förster resonance energy transfer (FRET)

ABSTRACT

In many cases light harvesting nanomaterials are commonly applied as photovoltaics as well as photocatalyst materials. However, such a dual use depends critically on the charge dynamics across the involved nanostructured interface. Here, we have investigated PbS-ZnO light harvesting assemblies (LHAs) that can lead to efficient photovoltaics. In contrast, their photocatalytic properties remain poor. We demonstrate that fundamental, ultrafast photoinduced charge separation and charge recombination processes at the semiconductor-semiconductor interface are key factors for the dual application of LHAs. In the course of our investigation we have synthesized and characterized the PbS-ZnO LHAs using high resolution transmission electron microscopy (HRTEM) and UV–vis absorption spectroscopy. Picosecond-resolved photoluminescence study has been employed to investigate the ultrafast interfacial charge transfer dynamics within the LHA upon photoexcitation. Picosecond-resolved PL-quenching of ZnO nanoparticles (NPs) show Förster Resonance Energy Transfer (FRET) from donor ZnO NPs to the acceptor PbS quantum dots (QDs) and the latter has been employed to confirm the proximity of PbS to the host ZnO with molecular resolution. The photocatalytic activity of PbS – ZnO LHAs is probed by monitoring the photoreduction of the test contaminant methylene blue (MB) and correlated with ultrafast spectroscopic studies on LHAs. This allows a conclusion on the role of ultrafast electron shuttling across the interface in making the electron unavailable for a reduction of MB. The prospective use of the LHAs in photovoltaics is investigated by photoelectrochemical studies where working electrodes of PbS-ZnO LHAs show higher photocurrents than that of bare ZnO NPs. This clearly indicates that the presence of an Indiumtinoxide (ITO) substrate provides directionality to the shuttling electrons at the PbS-ZnO interface. The exploration of interfacial carrier dynamics in PbS-ZnO LHAs will be helpful in improving the design and efficiency of future solar energy harvesting devices.

1. Introduction

Light harvesting through photocatalysis[1] (PC) and dye sensitized solar cells[2] (DSSC) are related to excited state charge transfer across nanostructured oxide surfaces. The former case consists of the absorption of photons at the oxide surfaces with the consequent generation of electron/hole pairs and eventual reduction/oxidation of adsorbed contaminant species. On the other hand in the latter case the photogenerated electron/hole pairs at the oxide surface migrate to the external circuit for photocurrent generation through an electrical load. Thus it is clear that a precise knowledge of excited state charge transfer across oxide surfaces, either naked or with adsorbed species, is important to fully understand the microscopic mechanism related to technologically important processes of PC and DSSC, both of which indeed have strong social impact. Technological advances in multiple areas from solar energy conversion (DSSC) to environmental remediation (PC) have been exploiting the exceptional properties of TiO_2 and ZnO.[3–5] However, one limitation of the oxide materials is the large band gap which renders clean solar energy driven processes inefficient. In order to sensitize the oxides in the visible light, several strategies have been studied. In photovoltaics, sensitization with visible light absorbing dyes is a prevalent solution.[2] In photocatalysis strategies include impurity doping[6,7] in addition to the dye sensitization[8,9] of the host oxide nanoparticles. In one of our recent studies, hematoporphyrin sensitized ZnO nanorods exhibit twin applications in efficient visible light photocatalysis (VLP) and DSSC.[10] As the stability of

* Corresponding author.
E-mail address: skpal@bose.res.in (S.K. Pal).

http://dx.doi.org/10.1016/j.solmat.2014.12.032
0927-0248/

an organic dye on a wide band gap oxide material is an issue, another approach beside the organic dye sensitization is to combine the material with a semiconductor that has a narrow band gap and an energetically high-lying conduction band.[11] In this direction, Kamat[12] and coworkers show photoinduced electron transfer from CdSe quantum dots (QDs) of different sizes to three unique metal oxide (TiO_2, ZnO and SnO_2) and suggest that in addition to electron transfer at the QD-metal oxide interface, other loss mechanisms play key roles in the determination of overall device efficiency.

Lead chalcogenides (mainly PbS and PbSe) are gaining research interest because of their unique photophysical properties such as tunable and broad spectral responses extending from the visible to near-IR regions,[13,14] high absorption coefficient,[15] long exciton lifetimes,[16,17] multiple exciton generation (MEG),[18–21] and hot carrier extraction.[22] In a survey of contemporary literature it appeared that PbS quantum dot sensitized solar cells are efficient to harvest light in the NIR region.[23,24] However, the works related to the use of the PbS sensitized nanomaterials for the photocatalysis application in the visible region, clearly indicate [25] that the material is sensitive in the visible (at light energy of 2.5 times higher than the band gap of QD) rather NIR region. Being in this regime, investigation of dynamical steps in the universality/limitation of such common applications of the nanomaterial in similar experimental conditions is the primary motive of the present study.

Here, we have synthesized and characterized the nanoscopic structure using high resolution transmission electron microscopy (HRTEM) of a well-known light-harvesting assembly (LHA), PbS QD sensitized ZnO nanoparticles (NPs) and their common applications in photocatalysis and solar cell. As both the parent materials ZnO and PbS have their intrinsic photoluminescence (PL) because of their defect states and band gap emission, respectively,[26,27] steady state spectroscopic studies on the LHA have been employed for the interfacial charge/energy migration. Picosecond-resolved PL-quenching of ZnO nanoparticles shows Förster Resonance Energy Transfer (FRET) from donor ZnO to the acceptor PbS revealing nanoconjugate of the parent materials in the LHA. Picosecond-resolved photoluminescence (PL) study have been employed to investigate the ultrafast interfacial charge transfer dynamics in the LHA upon photoexcitation. We have also applied the LHA for the potential use in photocatalysis and photovoltaic applications under illumination of a number of excitation wavelengths ranging from UV to VIS region. The difference in efficacies of the LHA in the PC and DSSC applications is rationalized from the crucial interfacial charge migration upon photoexcitation.

2. Experimental section

Analytical grade chemicals were used for synthesis without further purifications.

2.1. Synthesis of ZnO NPs

ZnO NPs were synthesized in a colloidal solution using ethanol, C_2H_5OH (Merck), as the solvent. The coprecipitation technique has been reported in previous publications from the group.[28–30] Briefly, 20 mL of 4 mM zinc acetate dihydrate, $(CH_3COO)_2Zn$, $2H_2O$ (Merck), solution was heated at 70 °C for 30 min. 20 mL of 4 mM sodium hydroxide, NaOH (Merck), solution in ethanol was then added and the mixture was hydrolyzed for 2 h at 60 °C to obtain NPs of average diameters of ~6 nm.

2.2. Sensitization of PbS QDs on ZnO NP surface

TOPO capped colloidal PbS QDs (EviDots from Evident technologies) in toluene were assembled to the ZnO NPs by constant stirring at room temperature in the dark for 12 h. After the sensitization process, the solution was centrifuged for a few minutes and the supernatant clear solution was removed. Then the sensitized material was washed with toluene several times. The LHA was then dried in a water bath and stored in the dark until further use.

2.3. Characterization methods

Transmission electron microscopy (TEM) grids were prepared by applying a diluted drop of the ZnO−PbS LHAs samples to carbon-coated copper grids. Particle sizes were determined from micrographs recorded at a magnification of 100000X using an FEI (Technai S-Twin, operating at 200 kV) instrument. For optical experiments, the steady-state absorption and emission were determined with a Shimadzu UV-2450 spectrophotometer and a Jobin Yvon Fluoromax-3 fluorimeter respectively. Picosecond-resolved spectroscopic studies were done using a commercial time correlated single photon counting (TCSPC) setup from Edinburgh Instruments (instrument response function (IRF=80 ps), excitation at 375 nm). The observed fluorescence transients were fitted by using a nonlinear least square fitting procedure to a function $\left(X(t) = \int_0^t E(t')R(t-t')dt'\right)$ comprising of convolution of the IRF (E(t)) with a sum of exponentials ($R(t) = A + \sum_{i=1}^{N} B_i e^{-t/\tau_i}$) with pre-exponential factors (B_i), characteristic lifetimes (τ_i) and a background (A). Relative concentration in a multi-exponential decay is finally expressed as, $c_n = B_n/(\sum_{i=1}^{N} B_i) \times 100$. The average lifetime (amplitude-weighted) of a multi-exponential decay is expressed as $\tau_{av} = \sum_{i=1}^{N} c_i\tau_i$.

2.4. Förster resonance energy transfer (FRET) calculations

In order to estimate FRET efficiency of the donor (ZnO) and hence to determine distance of donor-acceptor pairs, we used the following methodology.[31] The Förster distance (R_0) is given by,

$$R_0 = 0.211 \times [\kappa^2 n^{-4} Q_D J]^{\frac{1}{6}} \left(\text{in } \mathring{A}\right) \quad (1)$$

where, κ^2 is a factor describing the relative orientation in space of the transition dipoles of the donor and acceptor. For donor and acceptors that randomize by rotational diffusion prior to energy transfer, the magnitude of κ^2 is assumed to be 2/3. The refractive index (n) of the medium is assumed to be 1.496. Q_D, the integrated quantum yield of the donor in the absence of acceptor is measured to be 3.8×10^{-3} .J, the overlap integral, which expresses the degree of spectral overlap between the donor emission and the acceptor absorption, is given by,

$$J(\lambda) = \frac{\int_0^\infty F_D(\lambda)\varepsilon_A(\lambda)\lambda^4 d\lambda}{\int_0^\infty F_D(\lambda)d\lambda} \quad (2)$$

where, $F_D(\lambda)$ is the fluorescence intensity of the donor in the wavelength range of λ to $\lambda+d\lambda$ and is dimensionless; $\varepsilon_A(\lambda)$ is the extinction coefficient (in M^{-1} cm^{-1}) of the acceptor at λ. If λ is in nm, then J is in units of $M^{-1}cm^{-1}nm^4$. The estimated value of the overlap integral is 2.50×10^{15}. Once the value of R_0 is known, the donor-acceptor distance (r_{DA}) can be easily calculated using the formula,

$$r_{DA}^6 = \frac{[R_0^6(1-E)]}{E} \quad (3)$$

Here E is the efficiency of energy transfer. The transfer efficiency is measured using the relative fluorescence lifetime of

the donor, in absence (τ_D) and presence (τ_{DA}) of the acceptor.

$$E = 1 - \frac{\tau_{DA}}{\tau_D} \quad (4)$$

From the average lifetime calculation for the PbS-ZnO LHAs, we obtain the effective distance between the donor and the acceptor (r_{DA}), using Eqs. 3 and 4.

2.5. Photocatalysis measurement

For photocatalysis study, PbS-ZnO NCs were dispersed in DI water and aqueous solution of MB in DI water was used as test contaminant. A homemade UV source (8 W) along with high pass optical filters (320 nm and 475 nm) was used as a light source in this study. The mixture of photocatalyst and contaminant was irradiated for 1 h and the absorbance data were collected by ocean optics high resolution spectrometer through a computer interface. In all the cases, MB concentration was 5.4 mM and pH of the solution was 6.0. The percentage degradation (% DE) of MB was determined by using eq. 5:

$$\%\ DE = \frac{I_o - I}{I_o} \times 100 \quad (5)$$

where, I_0 is the initial absorption intensity of MB at λ_{max}= 660 nm and I is the absorption intensity after 1 h of continuous photoirradiation.

2.6. Photoelectrochemical measurements

Photoelectrochemical measurements were carried out in a three electrode cell with ZnO NPs and PbS-ZnO LHAs on ITO as working electrode, Pt wire as the counter electrode, Ag/AgCl as reference electrode and 0.5 mM aqueous NaOH solution as electrolyte. Data were obtained using a CH analyzer potentiostat (CHI1110C). The working electrode was irradiated with a Xenon light source (100 mW cm^{-2}).

3. Results and discussion

As illustrated in Fig. 1a, the representative high-resolution TEM (HRTEM) image of the PbS – ZnO LHA shows the average diameter is ~6 nm and ~3.2 nm for ZnO NPs and PbS QDs, respectively and confirms the proximity between PbS QDs and ZnO NPs. The synthesized ZnO NPs are spherical in shape and the NPs (diameter ~6 nm) do not show any quantum confinement effect as the Bohr radius of ZnO is ~3 nm. The lattice fringes of ZnO NPs and PbS QDs in PbS – ZnO LHAs are illustrated, which shows interplanar distances of ~0.314 and ~0.209 nm, corresponding to the spacing between two (1 0 0) planes[30] of ZnO NP and (2 2 0) planes[32] of PbS QD, respectively. In order to determine the complex formation between the TOPO-capped PbS QDs and ZnO NPs in the PbS – ZnO LHAs, we have also studied UV–vis spectroscopy, as shown in Fig. 1b. The bare ZnO NPs show absorption peak at 326 nm corresponding to the band-gap excitation, which is found to be red-shifted to 337 nm in PbS – ZnO LHAs. A bathochromic shift of ~11 nm in the absorption spectra can be attributed to the ground-state complex formation between PbS and ZnO NPs. The inset of Fig. 1b shows the absorption spectra of TOPO-capped PbS QDs.

As shown in Fig. 2a, the room temperature PL spectrum of ZnO NP is comprised of two emission bands upon excitation above the band-edge (λ_{ex}=300 nm).[30] The narrow UV band centered at 363 nm is due to the exciton recombination. The defect centers located near the surface are responsible for broad emission in blue green region which is composed of two bands, one arises from doubly charged vacancy center (V_o^{++}) located at 555 nm (P_2) and the other arises from singly charged vacancy center (V_o^{+}) located at

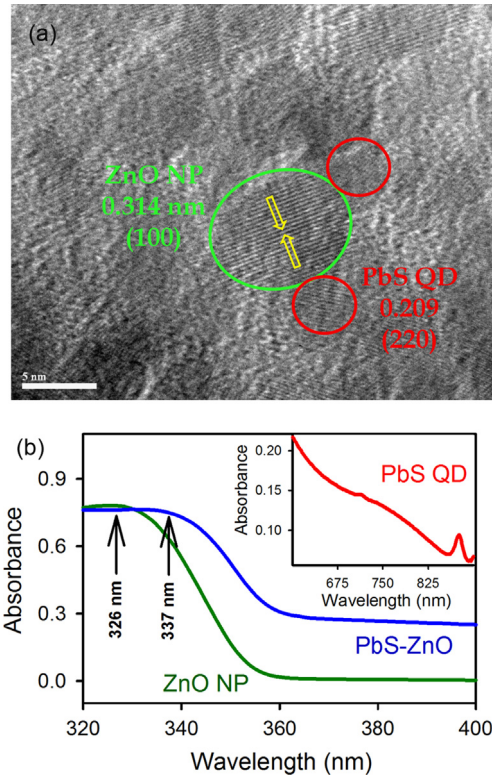

Fig. 1. (a) High-resolution TEM (HRTEM) image of PbS – ZnO LHA where PbS QD is attached to the ZnO NP surface. (b) UV–vis absorption spectra of bare ZnO NPs (dark green) and PbS – ZnO LHAs (blue). The inset shows the absorption spectra of PbS QDs (red).

500 nm (P_1).[33,34] For PbS – ZnO LHAs, there is a considerable decrease in the intensity of both the emission peaks as compared to the bare ZnO NPs. The decrease in emission intensities can be attributed to the efficient non-radiative photoinduced processes in PbS – ZnO interface. Herein, we propose Förster Resonance Energy Transfer (FRET) from the donor ZnO NPs to the acceptor PbS QDs in PbS-ZnO LHAs, which is responsible for the observed inhibition of the emission bands. The spectral overlap of the defect-mediated PL band of ZnO NPs with that of the PbS absorption is shown in Fig. 2a, inset. The fluorescence decay of bare ZnO NPs and PbS – ZnO LHAs were obtained upon excitation of 375 nm laser and monitored at 500 nm and 555 nm (Fig. 2b and c, respectively). The faster average excited state lifetime of the PbS-ZnO LHAs with respect to that of the ZnO NPs is clearly observed. The details of the spectroscopic parameters and the fitting parameters of the fluorescence decays are tabulated in Table 1. From FRET calculations, the distance between the donor and acceptor are determined to be 1.71 nm and 1.61 nm for P_1 and P_2 states, respectively. The calculated distances are consistent with the fact that the radius of the ZnO NPs used is ~3 nm and P_2 states are closer to the surface which leads to the shorter distance compare to the P_1 states. The energy transfer efficiency is calculated to be 81.6% and 86.3% from P_1 and P_2 states, respectively. The observation is in agreement with the reported literature that the P_2 state is in the proximity of the NP surface.[29,35] Further confirmation of non-radiative energy transfer from the ZnO NPs (donor) to the associated PbS QDs (acceptor) is evident from the emission characteristics of the acceptor as shown in Fig. 3. The excitation spectrum of the LHAs at the detection wavelength of 820 nm (acceptor emission) as shown in Fig. 3a clearly reveals a maximum at 360 nm, which is close to the absorption maximum of the ZnO NPs. The observation is consistent with the fact that the absorbed energy in the ZnO NPs migrate to the PbS QDs through a

non-radiative pathway.[36] In the case of FRET, it is expected that emission transient from the acceptor shows buildup in the time-scale comparable to the decay of the energy donor.[36] As shown in Fig. 3b, the emission transient of the acceptor PbS QDs reveal no apparent rise component. However, the shorter component of the lifetime of acceptor PbS QDs is significantly retarded in PbS-ZnO LHAs as shown in table 1 revealing an intrinsic buildup in the excited state due to FRET. We have estimated the buildup rate following reported procedure[12] and found to be $1.45 \times 10^7\ s^{-1}$, which is close to the FRET rate from donor ZnO NPs to acceptor PbS QDs ($1.47 \times 10^7\ s^{-1}$). The observation confirms the non-radiative energy transfer process from the donor ZnO NPs to the acceptor PbS QDs. As shown in Fig. 3b the overall quenching of the emission (steady state and transient) of PbS QDs in the LHAs clearly indicates that other non-radiative excited state events are associated following the energy transfer from the donor ZnO NPs. In order to investigate the non-radiative pathway of PbS QDs in the LHAs upon excitation, we have excited the nanocomposite at 510 nm and followed the steady and time-resolved emission as shown in Fig. 4. The quenching of the emission of the PbS QDs in the LHAs clearly reveals ultrafast (table 1) electron transfer from the excited QDs to the CB of ZnO NPs through non-radiative pathway.[37] A non radiative ultrafast decay of 40 ps revealing the charge migration from the excited PbS to the host ZnO NPs is evident from Fig. 4b. The manifestation of such charge transfer process in the emission of ZnO NPs at 540 nm upon excitation at 375 nm is also evident from Fig. 2d.

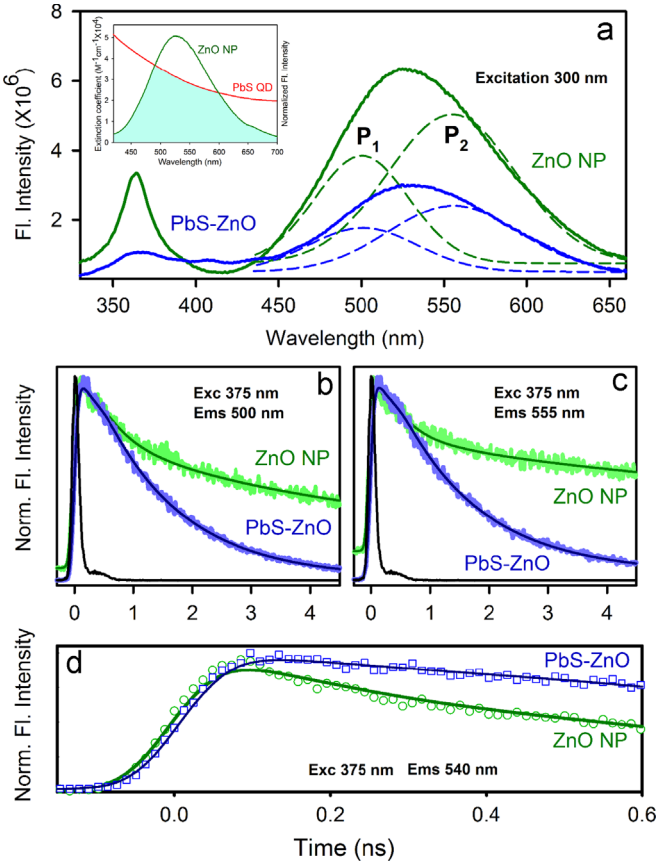

Fig. 2. (a) Room temperature PL spectra of ZnO NPs (dark green) and PbS – ZnO LHAs (blue) are shown. The excitation wavelength was at 300 nm. The broad emission band is composed of two components, P_1 (500 nm) and P_2 (555 nm). The inset shows the overlap of ZnO NP emission and PbS QD absorption. The picosecond-resolved fluorescence transients of ZnO NPs (excitation at 375 nm) in the absence (dark green) and in the presence of PbS QDs (red) collected at (b) 500 nm, (c) 555 nm and (d) 540 nm (shorter time window) are shown.

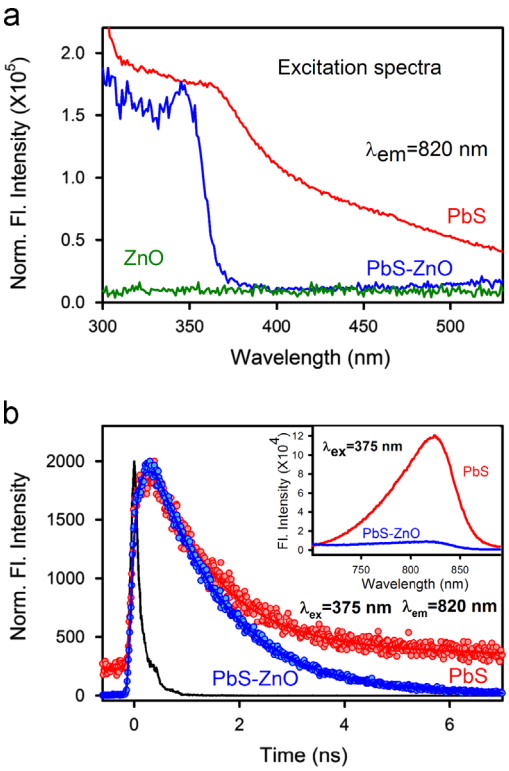

Fig. 3. (a) Excitation spectra of ZnO NPs (dark green), PbS QDs (red) and PbS – ZnO LHAs (blue) monitored at 820 nm. (b) The picosecond-resolved fluorescence transients of PbS QDs (excitation at 375 nm) in the absence (red) and in the presence of ZnO NPs (blue) collected at 820 nm. The inset shows the room temperature PL spectra of PbS QDs (red) and PbS – ZnO LHAs (blue) upon excitation at 375 nm.

Table 1
Dynamics of picosecond-resolved luminescence transients of ZnO NP, PbS-ZnO LHA and PbS QD[a]

Sample	Excitation wavelength (nm)	Detection wavelength (nm)	τ_1 (ns)	τ_2 (ns)	τ_3 (ns)	τ_{avg} (ns)
ZnO NP	375	500	0.46 ± 0.03 (43.8%)	4.52 ± 0.05 (41.6%)	37.39 ± 0.52 (14.6%)	7.55 ± 0.09
PbS-ZnO LHA	375	500	1.30 ± 0.05 (95.5%)	3.46 ± 0.24 (4.5%)		1.39 ± 0.03
ZnO NP	375	555	0.37 ± 0.03 (46.2%)	5.07 ± 0.12 (25%)	44.93 ± 0.37 (28.8%)	14.38 ± 0.14
PbS-ZnO LHA	375	555	1.32 ± 0.05 (94.3%)	5.22 ± 0.37 (4.5%)	42.29 ± 2.76 (1.2%)	1.98 ± 0.06
ZnO NP	375	540	0.38 ± 0.03 (75.3%)	3.36 ± 0.07 (17.2%)	38.64 ± 0.69 (7.5%)	3.76 ± 0.07
PbS-ZnO LHA	375	540	1.31 ± 0.03 (92.8%)	4.79 ± 0.51 (5.1%)	45.95 ± 2.7 (2.1%)	2.42 ± 0.12
PbS QD	375	820	1.17 ± 0.05 (91%)	13.21 ± 0.76 (9%)		2.25 ± 0.08
PbS-ZnO LHA	375	820	1.41 ± 0.05 (100%)			1.41 ± 0.03
PbS QD	510	820	130.35 ± 3.54 (100%)			130.35 ± 3.54
PbS-ZnO LHA	510	820	0.04 ± 0.03 (99.33%)	138.34 ± 8.71 (0.66%)		0.95 ± 0.058

[a] Numbers in the parenthesis indicate relative weightages.

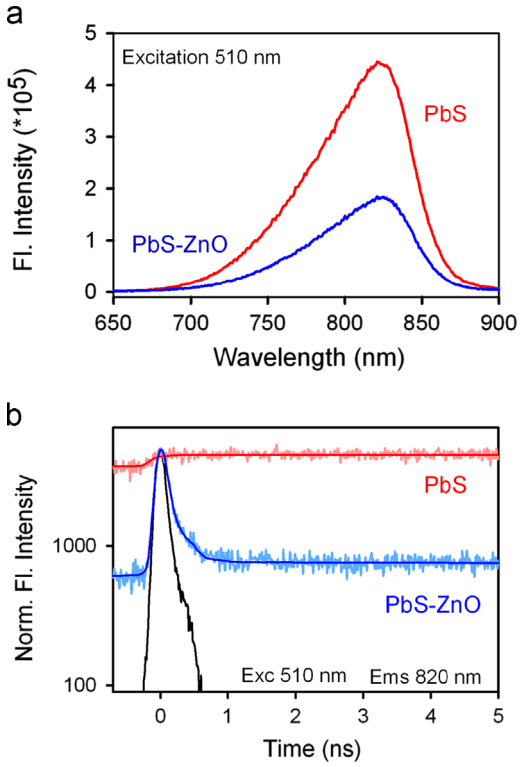

Fig. 4. (a) Room temperature PL spectra (excitation wavelength was at 510 nm) of PbS QDs (red) and PbS – ZnO LHAs (blue) are shown. (b) Fluorescence decay profiles of PbS QDs in the absence (red) and presence of ZnO NPs (blue) upon excitation at 510 nm and monitored at 820 nm.

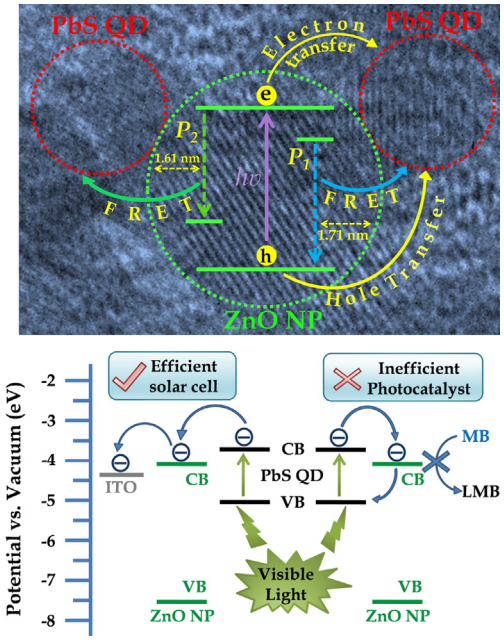

Scheme 1. Schematic presentation of the interfacial carrier dynamics in PbS-ZnO LHAs (Upper panel). Lower panel shows the schematic energy level diagram and charge transfer processes for photocatalysis and photovoltaic applications.

Table 1 reveals that the shorter component of the decay of bare ZnO NPs (0.46 ns and 0.37 ns for P_1 and P_2 states respectively) increases upon attaching to the PbS QDs (1.30 ns and 1.32 ns respectively). The lengthening of the faster relaxation times from the P_1 and P_2 states confirms the following two phenomena. Firstly, the quenching due to FRET is not operative in the time timescale of ~400 ps. Secondly, the recombination processes in the ZnO defect states are heavily retarded in the proximity of PbS QDs as clearly shown in Fig. 2d. The retardation of the recombination may be attributed to the quenching of the photoexcited holes of ZnO NPs by the PbS QDs. In an earlier study the proximity of a hole trapping molecule (4-amino-thiophenole) to CdSe QD is shown to increase the radiative recombination time of the QD at room temperature.[38] In our case the photo-generated hole in the valence band of the ZnO NPs is proposed to be quenched by an electron from the valence band of PbS QDs, which is expected to be recovered from the electron in the conduction band/P_1 state of the ZnO NPs (upper panel of scheme 1).

The room temperature PL spectra of PbS QDs shows emission peak at 820 nm upon the excitation at 510 nm, as shown in Fig. 4a. The intensity of the emission peak decreases considerably when the QDs are attached to the ZnO NPs. This is attributed to the efficient charge migration from the conduction band of PbS QD to the ZnO NPs.[16] The fluorescence decays (Fig. 4b) of PbS QDs and PbS – ZnO LHAs were measured upon excitation with 510 nm laser, and monitored at wavelength 820 nm. The emission decay curve of PbS QDs is fitted with single exponential function with a lifetime of 130.35 ns (Table 1). In case of PbS – ZnO LHA, the decay curve of PbS QD deviated from single exponential to bi-exponential showing one significant shorter lifetime 40 ps (99%) and a minor longer lifetime of 140 ns (1%). The observed decrease in lifetime could be correlated to the electron transfer process from PbS QDs to ZnO NPs.[16,39] Plass et al.[37] have investigated the electron transfer in a solar cell structure made by in situ growth of PbS QDs in a porous TiO_2 film, where initial charge separation occurs in 1 ps due to the electron trapping in PbS QD followed by electron injection into the conduction band of TiO_2 having a time constant of 20 ps. The band alignment of PbS QDs and ZnO NPs are well documented in the literature. The energy levels of photoexcited electrons and holes of 3.2 nm PbS QDs are at −3.7 and −5.1 eV[16] and the lowest unoccupied molecular orbital (LUMO) of ZnO NPs is −4.3 eV.[40] Eita et al.[41] have shown that the electron injection from photoexcited PbS QDs to ZnO NPs over ITO plate occurs on a time scale of a few hundred femtoseconds and the observation is supported by the interfacial electronic-energy alignment between the donor and acceptor moieties.

In order to investigate the interfacial charge transfer dynamics in photocatalysis application, we have probed the methylene blue (MB) reduction in presence of the LHA in aqueous solution. For the preferential excitation, we have used 475 nm high pass (HP) optical filter placed on a home-made UV bath (8 W) before the sample. The results for the photoreduction of MB are shown in Fig. 5a. The photoreduction of MB implies the generation of the colorless photoproduct Leuco-Methylene Blue (LMB). The maximum photoreduction is observed in the presence of ZnO NPs under UV irradiation while using 475 HP optical filter no photoreduction of MB is observed. This is obvious because ZnO being a wide band gap (3.37 eV) semiconductor, the band-gap excitation occurs only at wavelengths less than 380 nm. However, ZnO NPs in the proximity of PbS QDs in the LHAs show inefficient MB photoreduction both in presence and absence of the HP filter. We have attributed the de-excitation of ZnO NPs through FRET to be responsible for the less photocatalytic activity of the LHAs in UV light excitation (no filter) as shown in the upper panel of Scheme 1. On the other hand visible light excitation (with filter) of the PbS QDs in the LHAs shuttles the photogenerated electron in the QDs through the conduction band of the ZnO NPs as shown in lower panel of Scheme 1. Overall for white light excitation of the LHAs, the photogenerated electron is sparsely available for the reduction of MB in the solution due to the above mentioned two ultrafast mechanisms.

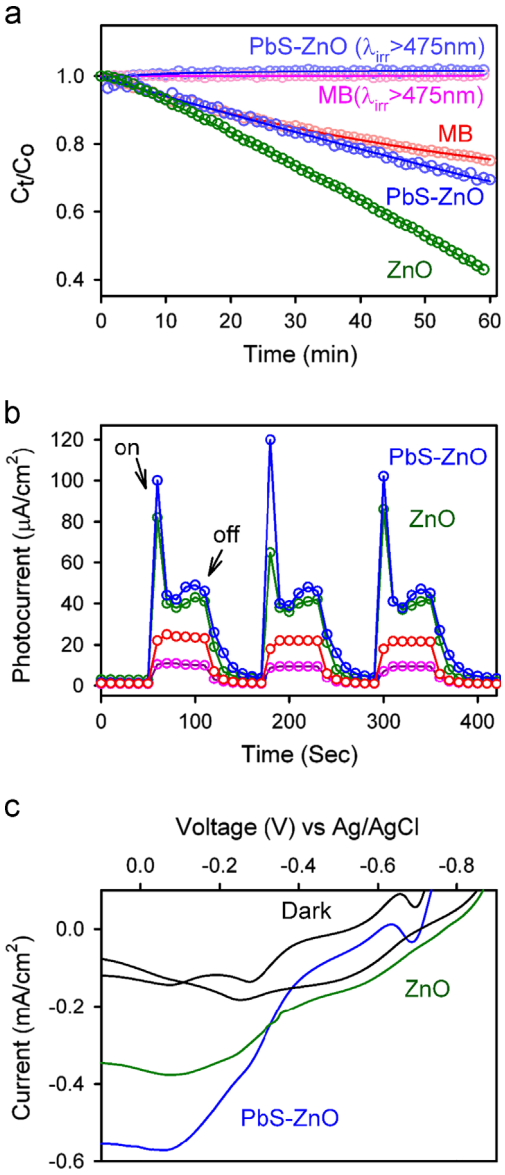

Fig. 5. **(a)** Photocatalytic degradation of MB in the presence of PbS QDs (blue), ZnO NPs (red and dark red) and PbS−ZnO LHA (dark green and pink) under different irradiation conditions (the optical filters used for the desired irradiation are indicated in the parentheses). (b) Photocurrent response of PbS-ZnO LHA (blue) and ZnO (green) under 100 mW cm^{-2} incident power irradiation and PbS-ZnO (red) and ZnO (pink) under visible light irradiation (using 400 nm filter) without any bias voltage. (c) Photocurrent-voltage (I-V) characteristics of PbS-ZnO LHA (blue) and ZnO (green) under 100 mW cm^{-2} incident power irradiation.

In order to investigate the efficacy of PbS-ZnO LHAs in photovoltaic application, we have performed photoelectrochemical measurements in a half cell geometry using the LHAs on ITO plate as anode and Pt as counter electrode.[42] For I-V measurement, the Ag/Ag^{+} couple are used as reference electrode. The photocurrent measurement of ZnO and PbS-ZnO LHAs were carried out in order to better understand the electron transfer processes in terms of short circuit current. The light source (100 mW cm^{-2}) was turned on and off every 60 s and the obtained photocurrent values were continuously recorded. As shown in Fig. 5b, under full light illumination PbS-ZnO has greater photocurrent response than ZnO NPs on the ITO plate. The observation is consistent with the fact that the LHAs would able to harvest a wide band of light spectrum from UV to NIR in contrast to the ZnO NPs, which is expected to harvest only UV region of the incident white light. The initial spike is observed due to the slower recovery of the photoexcited holes from the electrolytes and is consistent with other studies reported in the literature.[42] Significant enhancement of the photocurrent in presence of PbS in the proximity of ZnO NPs in contrast to the retardation of photocatalysis activity of the LHAs is rationalized in the following way. The photogenerated electron in the PbS as well as ZnO NPs is expected to be channelized to the ITO plate because of the lower potential as shown in lower panel of Scheme 1. The I-V characteristics of the LHAs in presence of white light as shown in Fig. 5c reveals significantly higher short-circuit current compared to those of the ZnO NPs. The observation clearly indicates the importance of the presence of ITO plate in the interfacial carrier dynamics of PbS-ZnO LHAs in photovoltaic application.

4. Conclusion

We have investigated dynamical processes in PbS-ZnO light harvesting assemblies upon photoexcitation and their common applications in photocatalysis and photovoltaics. The picosecond-resolved PL-quenching of ZnO nanoparticles in the presence of PbS quantum dots shows Förster Resonance Energy Transfer (FRET) from donor ZnO NPs to the acceptor PbS QDs and has been employed to confirm molecular proximity. Picosecond-resolved time correlated single photon counting (TCSPC) shows the ultrafast quenching of photoexcited holes in the ZnO NPs by PbS QDs. The photocatalytic activity of PbS−ZnO LHAs is probed by monitoring the photoreduction of the test contaminant methylene blue (MB). This shows that the LHA is inefficient as a photocatalyst because the photoexcited electrons shuttle across the semiconductor-semiconductor interface and are unavailable to the MB. The prospective use of the LHAs in photovoltaics is investigated by the photoelectrochemical studies where PbS-ZnO LHAs as working electrode shows higher photocurrent than that of bare ZnO NPs. This clearly indicates that the presence of ITO substrate provides directionality to the shuttling electrons at the PbS-ZnO interface. Thus PbS-ZnO LHAs are efficient in solar cell applications but are inefficient in heterogeneous catalysis. The exploration of interfacial carrier dynamics in PbS-ZnO LHAs will be helpful in improving the design and efficiency of the future solar energy harvesting devices.

Acknowledgments

P.K. thanks CSIR (India) for fellowship. We thank DST (India) for financial grants DST/TM/SERI/2k11/103 and SB/S1/PC-011/2013. We also thank DAE (India) for financial grant, 2013/37P/73/BRNS. PL thanks the NTH-School “Contacts in Nanosystems” and the Braunschweig International Graduate School of Metrology.

References

[1] A. Fujishima, K. Honda, Electrochemical photolysis of water at a semiconductor electrode, Nature 238 (1972) 37–38.
[2] B. O'Regan, M. Gratzel, A low-cost, high-efficiency solar cell based on dye-sensitized colloidal TiO2 films, Nature 353 (1991) 737–740.
[3] S. Sardar, S. Sarkar, M.T.Z. Myint, S. Al-Harthi, J. Dutta, S.K. Pal, Role of central metal ions in hematoporphyrin-functionalized titania in solar energy conversion dynamics, Phys. Chem. Chem. Phys. 15 (2013) 18562–18570.
[4] A. Hagfeldt, M. Grätzel, Molecular photovoltaics, Acc. Chem. Res. 33 (2000) 269–277.
[5] M.R. Hoffmann, S.T. Martin, W. Choi, D.W. Bahnemann, Environmental applications of semiconductor photocatalysis, Chem. Rev. 95 (1995) 69–96.
[6] C. Chen, X. Li, W. Ma, J. Zhao, H. Hidaka, N. Serpone, Effect of transition Metal ions on the TiO2-assisted photodegradation of dyes under visible irradiation: a probe for the interfacial electron transfer process and reaction mechanism, J. Phys. Chem. B 106 (2001) 318–324.
[7] R. Asahi, T. Morikawa, T. Ohwaki, K. Aoki, Y. Taga, Visible-light photocatalysis in nitrogen-doped titanium oxides, Science 293 (2001) 269–271.

[8] W. Zhao, Y. Sun, F.N. Castellano, Visible-light induced water detoxification catalyzed by PtII dye sensitized titania, J. Am. Chem. Soc. 130 (2008) 12566–12567.
[9] E. Bae, W. Choi, Highly enhanced photoreductive degradation of perchlorinated compounds on dye-sensitized metal/TiO2 under visible light, Environ. Sci. Technol. 37 (2002) 147–152.
[10] S. Sarkar, A. Makhal, T. Bora, K. Lakhsman, A. Singha, J. Dutta, S.K. Pal, Hematoporphyrin–ZnO nanohybrids: twin applications in efficient visible-light photocatalysis and dye-sensitized solar cells, ACS Appl. Mater. Interfaces 4 (2012) 7027–7035.
[11] P.V. Kamat, Quantum dot solar cells. semiconductor nanocrystals as light harvesters†, J. Phys. Chem. C 112 (2008) 18737–18753.
[12] K. Tvrdy, P.A. Frantsuzov, P.V. Kamat, Photoinduced electron transfer from semiconductor quantum dots to metal oxide nanoparticles, Proc. Natl. Acad. Sci 108 (2011) 29–34.
[13] V.I. Klimov, A.A. Mikhailovsky, S. Xu, A. Malko, J.A. Hollingsworth, C.A. Leatherdale, H.-J. Eisler, M.G. Bawendi, Optical gain and stimulated emission in nanocrystal quantum dots, Science 290 (2000) 314–317.
[14] M.A. Hines, G.D. Scholes, Colloidal PbS nanocrystals with size-tunable near-infrared emission: observation of post-synthesis self-narrowing of the particle size distribution, Adv. Mater. 15 (2003) 1844–1849.
[15] L. Cademartiri, E. Montanari, G. Calestani, A. Migliori, A. Guagliardi, G.A. Ozin, Size-dependent extinction coefficients of PbS quantum dots, J. Am. Chem. Soc. 128 (2006) 10337–10346.
[16] B.-R. Hyun, Y.-W. Zhong, A.C. Bartnik, L. Sun, H.D. Abruña, F.W. Wise, J.D. Goodreau, J.R. Matthews, T.M. Leslie, N.F. Borrelli, Electron injection from colloidal PbS quantum dots into titanium dioxide nanoparticles, ACS Nano 2 (2008) 2206–2212.
[17] H.C. Leventis, F. O'Mahony, J. Akhtar, M. Afzaal, P. O'Brien, S.A. Haque, Transient optical studies of interfacial charge transfer at nanostructured metal oxide/PbS quantum dot/organic hole conductor heterojunctions, J. Am. Chem. Soc. 132 (2010) 2743–2750.
[18] J.J.H. Pijpers, R. Ulbricht, K.J. Tielrooij, A. Osherov, Y. Golan, C. Delerue, G. Allan, M. Bonn, Assessment of carrier-multiplication efficiency in bulk PbSe and PbS, Nat. Phys. 5 (2009) 811–814.
[19] J.A. McGuire, M. Sykora, J. Joo, J.M. Pietryga, V.I. Klimov, Apparent versus true carrier multiplication yields in semiconductor nanocrystals, Nano Lett. 10 (2010) 2049–2057.
[20] M.C. Beard, A.G. Midgett, M.C. Hanna, J.M. Luther, B.K. Hughes, A.J. Nozik, Comparing multiple exciton generation in quantum dots to impact ionization in bulk semiconductors: implications for enhancement of solar energy conversion, Nano Lett. 10 (2010) 3019–3027.
[21] A.A.O. El-Ballouli, E. Alarousu, A. Usman, J. Pan, O.M. Bakr, O.F. Mohammed, Real-time observation of ultrafast intraband relaxation and exciton multiplication in PbS quantum dots, ACS Photonics 1 (2014) 285–292.
[22] W.A. Tisdale, K.J. Williams, B.A. Timp, D.J. Norris, E.S. Aydil, X.-Y. Zhu, Hot-electron transfer from semiconductor nanocrystals, Science 328 (2010) 1543–1547.
[23] H.J. Lee, P. Chen, S.-J. Moon, F. Sauvage, K. Sivula, T. Bessho, D.R. Gamelin, P. Comte, S.M. Zakeeruddin, S.I. Seok, M. Grätzel, M.K. Nazeeruddin, Regenerative PbS and CdS quantum dot sensitized solar cells with a cobalt complex as hole mediator, Langmuir 25 (2009) 7602–7608.
[24] O.E. Semonin, J.M. Luther, M.C. Beard, Quantum dots for next-generation photovoltaics, Mater. Today 15 (2012) 508–515.
[25] C. Wang, K.-W. Kwon, M.L. Odlyzko, B.H. Lee, M. Shim, PbSe Nanocrystal/TiOx heterostructured films: simple route to nanoscale heterointerfaces and photocatalysis, J. Phys. Chem. C 111 (2007) 11734–11741.
[26] T. Bora, K.K. Lakshman, S. Sarkar, A. Makhal, S. Sardar, S.K. Pal, J. Dutta, Modulation of defect-mediated energy transfer from ZnO nanoparticles for the photocatalytic degradation of bilirubin, Beilstein J. Nanotechnol 4 (2013) 714–725.
[27] D. Deng, J. Xia, J. Cao, L. Qu, J. Tian, Z. Qian, Y. Gu, Z. Gu, Forming highly fluorescent near-infrared emitting PbS quantum dots in water using glutathione as surface-modifying molecule, J. Colloid Sci. 367 (2012) 234–240.
[28] S. Sarkar, A. Makhal, S. Baruah, M.A. Mahmood, J. Dutta, S.K. Pal, Nanoparticle-sensitized photodegradation of Bilirubin and potential therapeutic application, J. Phys. Chem. C 116 (2012) 9608–9615.
[29] A. Makhal, S. Sarkar, T. Bora, S. Baruah, J. Dutta, A.K. Raychaudhuri, S.K. Pal, Dynamics of light harvesting in ZnO nanoparticles, Nanotechnology 21 (2010) 265703.
[30] S. Sarkar, A. Makhal, T. Bora, S. Baruah, J. Dutta, S.K. Pal, Photoselective excited state dynamics in ZnO-Au nanocomposites and their implications in photocatalysis and dye-sensitized solar cells, Phys. Chem. Chem. Phys. 13 (2011) 12488–12496.
[31] J.R. Lakowicz, Principles of Fluorescence Spectroscopy, second ed., Kluwer Academic/ Plenum, New York, 1999.
[32] M. Flores-Acosta, M. Sotelo-Lerma, H. Arizpe-Chávez, F.F. Castillón-Barraza, R. Ramírez-Bon, Excitonic absorption of spherical PbS nanoparticles in zeolite A, Solid State Commun. 128 (2003) 407–411.
[33] A. van Dijken, E.A. Meulenkamp, D. Vanmaekelbergh, A. Meijerink, The kinetics of the radiative and nonradiative processes in nanocrystalline ZnO particles upon photoexcitation, J. Phys. Chem. B 104 (2000) 1715–1723.
[34] K. Vanheusden, W.L. Warren, C.H. Seager, D.R. Tallant, J.A. Voigt, B.E. Gnade, Mechanisms behind green photoluminescence in ZnO phosphor powders, J. Appl. Phys. 79 (1996) 7983–7990.
[35] S. Sarkar, S. Sardar, A. Makhal, J. Dutta, S. Pal, Engineering FRET-based solar cells: manipulation of energy and electron transfer processes in a light harvesting assembly, in: X. Wang, Z.M. Wang (Eds.), High-Efficiency Solar Cells, Springer International Publishing, Switzerland, 2014, pp. 267–318.
[36] S.S. Narayanan, S.S. Sinha, S.K. Pal, Sensitized emission from a chemotherapeutic drug conjugated to CdSe/ZnS QDs, J. Phys. Chem. C 112 (2008) 12716–12720.
[37] R. Plass, S. Pelet, J. Krueger, M. Grätzel, U. Bach, Quantum dot sensitization of organic – inorganic hybrid solar cells, J. Phys. Chem. B 106 (2002) 7578–7580.
[38] C. Burda, S. Link, M. Mohamed, M. El-Sayed, The relaxation pathways of CdSe nanoparticles monitored with femtosecond time-resolution from the visible to the IR: assignment of the transient features by carrier quenching, J. Phys. Chem. B 105 (2001) 12286–12292.
[39] S.M. Willis, C. Cheng, H.E. Assender, A.A.R. Watt, The transitional heterojunction behavior of PbS/ZnO colloidal quantum dot solar cells, Nano Lett. 12 (2012) 1522–1526.
[40] Y. Liang, T. Novet, J.E. Thorne, B.A. Parkinson, Photosensitization of ZnO single crystal electrodes with PbS quantum dots, Phys. Status Solidi A 211 (2014) 1954–1959.
[41] M. Eita, A. Usman, A.a.O. El-Ballouli, E. Alarousu, O.M. Bakr, O.F. Mohammed, A layer-by-layer ZnO nanoparticle–PbS quantum dot self-assembly platform for ultrafast interfacial electron injection, Small (2014), http://dx.doi.org/10.1002/smll.201400939.
[42] I. Robel, V. Subramanian, M. Kuno, P.V. Kamat, Quantum dot solar cells. Harvesting light energy with CdSe nanocrystals molecularly linked to mesoscopic TiO2 films, J. Am. Chem. Soc. 128 (2006) 2385–2393.